# CTF VALIDATION ACTIVITIES

**T. Blyth, C. Dances, M. Avramova**
Department of Mechanical and Nuclear Engineering
The Pennsylvania State University
137 Reber Building, University Park, PA, 16802
tyb5095@psu.edu, cad39@psu.edu, mna109@psu.edu

**R. Salko**
Oak Ridge National Laboratory
Oak Ridge, TN, 37831
salkork@ornl.gov

## ABSTRACT

The Reactor Dynamics and Fuel Management Group (RDFMG) at The Pennsylvania State University (PSU) has become active in the Consortium for Advanced Simulation of Light Water Reactors (CASL) program by delivering, supporting, and further developing CTF, the PSU version of the COolant Boiling in Rod Arrays - Two Fluids (COBRA-TF) Thermal/Hydraulic (T/H), sub-channel program. CTF is an advanced transient code based on separated two-phase flow representation. The code includes a wide range of thermal-hydraulic models important to Light Water Reactor (LWR) safety analysis. Recent CTF improvements and developments include pre- and post-processing capabilities as well as code optimization, leading to significantly reduced memory consumption and faster execution time.

To provide a sufficient level of certainty and confidence in the predictive capabilities of the code for the scenarios it was designed to model - rod bundle geometries with operating conditions that are representative of prototypical LWRs in both normal and accident conditions - the code was subjected to an extensive validation program. This was performed by modeling a variety of experiments that simulate these scenarios and then presenting a qualitative and quantitative analysis of the results that demonstrates the accuracy to which CTF is capable of capturing specific quantities of interest. These include pressure drop, void content, departure from nucleate boiling, turbulent mixing and void drift, and heat transfer.

The paper will present CTF applications to several experiments including the international OECD/NRC Boiling Water Reactor Full-Size Fine-Mesh Bundle Test (BFBT) and Pressurized Water Reactors Subchannel and Bundle Tests (PSBT) benchmarks; the Pacific Northwest National Laboratory (PNNL) free- and forced-convection 2x6 tests; Combustion Engineering (CE) 5x5 critical heat flux tests; the General Electric (GE) 3x3 void distribution tests; and the FRIGG data for single- and two-phase pressure drop, void distribution, and burnout in natural and forced circulation.

The CTF validation activities are performed following the CASL Validation and Uncertainty Quantification (VUQ) Strategy.

*Key Words*: CTF, CASL, Validation

## 1 INTRODUCTION

Modeling and simulating a physical system or the phenomena within is a complex process involving several steps. Formulating a mathematical model that suitably describes the physics being modeled is a first step. Determining an appropriate method to solve that mathematical model, and finally, translating all these steps into machine language in the form of a computer program to make the method useful for

solving real problems are also challenges. Additionally, each of these steps---model selection, assumptions, and coding---must be thoroughly tested and documented so as to instill confidence in the user that the resulting product is capable of performing its intended purpose. Ideally, good code documentation should inform the user: 1) what the code does, 2) how the code works, 3) how to use the code, and 4) that the code works as advertised [1].

Currently, the CTF documentation suite includes both a User Manual [2] and a Theory Manual [10], which address items 2 and 3 on the list. This work, while not a part of the documentation suite, will give insight on items 1 and 4. Furthermore, it is based on reference [1] which contains detailed data and discussion pertaining to items 1 and 4. Note that Item 4 covers code testing, which is a broad topic that ideally includes both verification and validation tasks. Whereas verification tasks demonstrate that the mathematical equations are being solved correctly and were implemented into the code in a bug-free way, validation tasks demonstrate that the correct equations are being solved, resulting in good agreement with experimental data. Comparing with experimental data is a necessary part of validation work. This paper briefly discusses part of the testing process to which CTF is subjected---validation testing. An important aspect of this validation suite is its tight integration in the CASL version of CTF. All of the tests created as part of this study have been included directly in the CTF code repository. Additionally, many of the tests are used as code regression tests that are run on a regular basis in automatic fashion. Due to the automated nature of the testing process, it is possible for the user to re-run the validation suite at the "push of a button". This helps to keep this validation study relevant during ongoing development activities in the code.

As user input values, CTF accepts boundary conditions including pressure, inlet temperature/enthalpy, radial and axial power distributions, and flow rates. Subchannel and rod geometry is entirely controlled by the user and can be manipulated to create complex sections and geometries as needed. Users can provide forcing functions for these boundary conditions in the event of a transient simulation. CTF utilizes a two-fluid three-field approach with 9 conservation equations. Many CTF modeling options are available to users. Spacer grid loss coefficients can be specified on a per-subchannel basis and there are turbulent mixing models which can be controlled as well. CTF adapts its own models based on parameters such as the flow regime and uses appropriate correlations for each region.

## 2 TEST DESCRIPTIONS

The basic design and purpose of each experiment are briefly discussed in this section. These are all experiments performed by reputable organizations where produced data are relevant and valuable. Additional information on each specific experimental design can be found in the respective references.

### 2.1 PSBT

The OECD (Organization for Economic Co-operation and Development) /NRC (US Nuclear Regulatory Commission) PWR Subchannel and Bundle Tests (PSBT) Benchmark includes both single-channel and rod-bundle geometries in steady-state and transient operating conditions. For this work, the rod bundles from the steady-state void distribution benchmark are examined. These are run with a 5x5 typical-length rod bundle complete with electrically-heated rods and 17 spacer grids. Many experiments were run with an array of axial/radial power and power/flow/pressure boundary conditions in order to produce a range of meaningful data for thermal-hydraulic codes to simulate. Temperature and void fraction measurements were taken at the exit of the subchannels. Please see reference [4] for further details about the PSBT Benchmark.

### 2.2 BFBT

Similar to the PSBT test cases, the geometry used in the OECD/NRC BWR Full-Size Fine-Mesh Bundle Test (BFBT) Benchmark in this document are 8x8 electrically-heated rod bundles from the

steady-state pressure drop benchmark as part of the critical power section. There are pressure taps along the heated length which are used to measure pressure losses across various axial spans. Seven spacer grids and a central, large, unheated water rod are also features of these tests. Please see reference [3] for a diagram of the pressure drop tap locations and further details about the BFBT Benchmark.

## 2.3 PNNL 2x6

An experiment was carried out at the Pacific Northwest National Laboratory (PNNL) utilizing a 2x6 rod array in order to provide insight to the effects of buoyancy on a reactor's flow patterns. Only the left half of the rod array, rods #1-6 as shown in Figure 1, was heated, causing natural convection temperature gradients to distribute flow across the bundle. There were several windows spaced along the heated length that allowed for laser readings of velocities. The heated length of the rods was 4 feet with an additional 6 inches on either side of unheated length. Temperatures were also recorded at these locations. Figure 1 shows the atypical layout (top view) of the test section and the 21 subchannels. Please see references [5, 6] for more details on the geometry and boundary conditions of this test case.

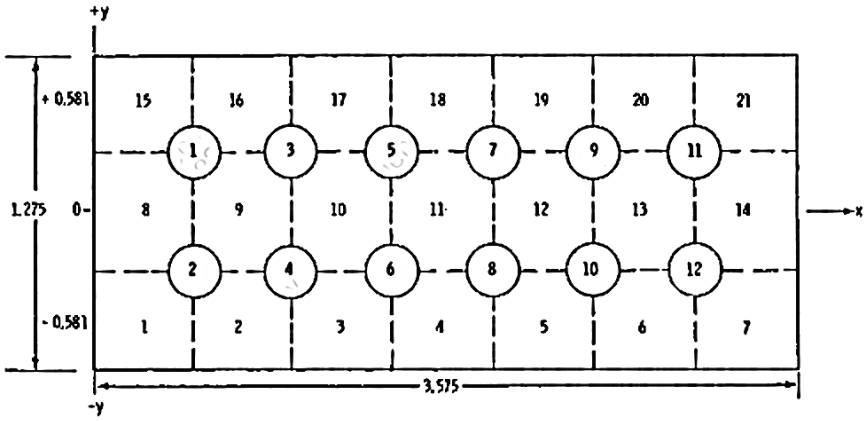


**Figure 1. PNNL 2x2 cross-section geometry**

## 2.4 CE 5x5

The Combustion Engineering (CE) 5x5 tests involved running over 70 tests of varying operating conditions on a 5x5, 7-foot tall electrically heated rod bundle facility. These tests were performed partially as a study into crud growth and the resulting fuel failures. The simulated bundles are representative of peripheral fuel assemblies as this was where the heavy crud deposits were noted. The operating conditions were varied such that heat transfer mechanisms in the bundle ranged from single-phase convection to saturated boiling using pressures of up to 2250 psi. Instrumentation included thermocouples fixed to the interior of two of the heater rods. Pressure drop measurements were also taken. Please see reference [7] for more geometry and boundary conditions details for these CE test cases.

## 2.5 GE 3x3

A 3x3 heated tube geometry was used in a BWR-like simulation with General Electric (GE) rods. The 16 subchannels were analyzed for their exit quality, mass flux, and enthalpies. These values were determined by blocking off each subchannel with ducting and using flowmeters (for mass flux) and heat balances (for enthalpy). Pressure losses were also taken using transducers spaced across the entire bundle. There are several spacer grids which consist of cylindrical pins fixing the rods in their positions. A wide range of power and inlet subcooling conditions were performed during the experimentation. Please see reference [8] for more details on the geometry and boundary conditions for these GE test cases.

## 2.6 FRIGG

The FRIGG test facility is unique with its circular rod lattice. It is modeled after the Marviken reactor assemblies and was used to verify the safety criteria of these reactors. Experiments included single- and two-phase pressure drop measurements, void distribution measurements, and burnout in both natural and forced circulation. The rods placed on three concentric rings of the geometry are shown in Figure 2. Modeling this type of geometry requires some careful calculations when meshing in CTF. As can be seen, four channels were utilized to create the model. The rods were also lumped together by section in order to create four rods for CTF's input. This is possible due to the equal gap lengths for each rod in a given ring. The wetted perimeter and cross-flow areas of each subchannel could then be carefully calculated using the new rod geometry. Please see reference [9] for more details on the FRIGG geometry and boundary conditions.

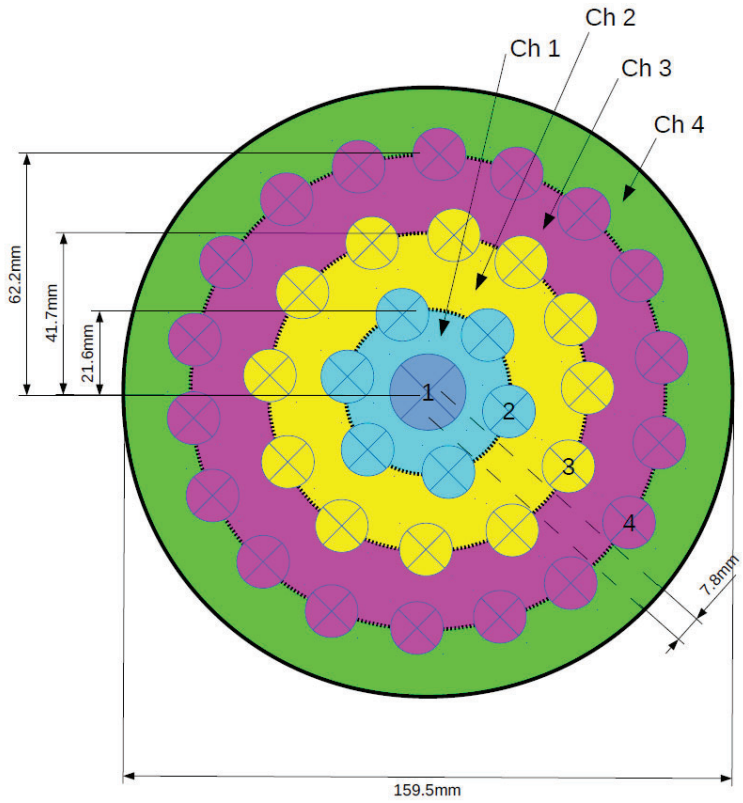


**Figure 2. FRIGG rod geometry**

# 3 EFFECTS TESTING

## 3.1 Comparison Metrics

Various experiments were modeled using CTF in order to compare numerical results with measured data. Different metrics were used to compare CTF's results with the experimental results. Utilizing statistical definitions allows for a way to quantize the accuracy of CTF in predicting various Quantities Of Interest (QOIs). The sample mean and standard deviation are most commonly employed to give a comparison between the predicted and measured values.

To compare differences in results, the root-mean-square error (RMSE) is employed as shown in Equation (1). It is slightly different than the standard deviation in that it compares simulated and measured points directly and then averages the sum of the difference squared.

$$\text{RMSE} = \sqrt{\frac{1}{N}\Sigma_{i=1}^{N}\left(x_{ctf,i} - x_{m,i}\right)^2} \quad (1)$$

Using relative root-mean-square (rRMS) is a method to remove the sampled quantity's units. It utilizes a relative error ratio by dividing by the measured value as shown in Equations (2) and (3).

$$\text{E}_{\text{rel}} = \frac{x_{measured} - x_{predicted}}{x_{measured}} \quad (2)$$

$$\text{rRMS} = \sqrt{\frac{1}{N}\Sigma_{i=1}^{N}E_{rel,i}^2} \quad (3)$$

## 3.2 Pressure Drop

CTF-calculated values of pressure drop take acceleration, frictional, and gravitational components into account. The sources of pressure drop are not always broken down in the experimental data, so the total pressure drop, shown in Equation (7), is often used as a metric for comparison. The components of the pressure drop are provided in Equation (4) through Equation (6).

$$\Delta P_{accel} = \left(\frac{\text{G}_\text{m}^2}{\rho_m^+}\right)_{out} - \left(\frac{\text{G}_\text{m}^2}{\rho_m^+}\right)_{in} \quad (4)$$

where the momentum flux term is:

$$\frac{\text{G}_\text{m}^2}{\rho_m^+} = \rho_v\alpha_v v_v^2 + \rho_l\alpha_l v_l^2 + \rho_l\alpha_d v_d^2 \quad (5)$$

and the gravity term is:

$$\Delta P_{gravity} = \rho_{mix} g \Delta X \quad (6)$$

$$\Delta P_{total} = \Delta P_{accel} + \Delta P_{friction} + \Delta P_{gravity} \quad (7)$$

### 3.2.1 BFBT

Within the BFBT experiments there are single-phase (Series 7) and two-phase (Series 6) pressure drop experiments against which CTF results are compared. For the 10 single-phase test cases of Series 7, CTF results were evaluated at each of the nine pressure tap locations found in the BFBT geometry. The RMSE and rRMS (in kPa and %, respectively) are calculated against the measured values in order to show CTF's effectiveness in predicting single-phase BWR-type pressure drops with spacer grids present in the flow. These results are shown in Table I.

**Table I. RMSE and rRMS for the BFBT Series 7 single-phase pressure drop results**

| Pressure Tap | RMSE [kPa] | rRMS [%] |
|---|---|---|
| dp301 | 0.097 | 6.8 |
| dp302 | 0.056 | 3.3 |
| dp303 | 0.188 | 7.5 |
| dp304 | 0.078 | 10.0 |
| dp305 | 0.087 | 8.1 |
| dp306 | 0.121 | 6.6 |
| dp307 | 0.326 | 5.2 |
| dp308 | 0.050 | 1.6 |
| dp309 | 0.364 | 3.9 |
| Total | 0.188 | 6.4 |

For reference, the experimental uncertainty in pressure drop is stated as 1% [3]. These nine pressure tap locations are spaced axially along the bundle, and some pressure drop measurements cover multiple spacer grids while others contain a single grid. This causes some discrepancies in the comparison results as a measurement over more grid spans would be expected to carry more uncertainty. This is shown in the RMSE column of Table I, but the rRMS column is able to account for the average relative error at each tap location and provide more meaningful results. These results are generally well outside of the 1% experimental errors which indicates there is room for model refinement inside CTF. Figure 3 shows the measured-to-predicted ratios of the single-phase tests plotted against the Reynolds number from each of the ten single-phase cases. This shows a slight trend of increasing accuracy as the Reynolds number increases.

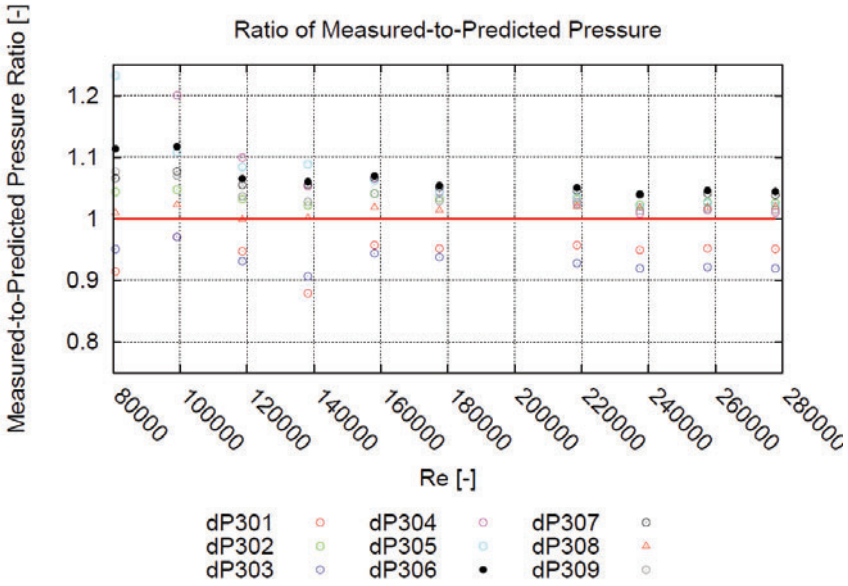


**Figure 3. BFBT Series 7 single-phase pressure drop ratios vs. Reynolds number**

For the two-phase pressure drops of BFBT Series 6 there are 18 test cases which use the same bundle geometry as the single-phase portion. Several pressure taps in this test series span regions in the bundle which contain higher void fractions and therefore increased computational complexity. The results for the RMSE and rRMS in Table II show that the upper-most spans do have the highest prediction error in CTF. The remaining pressure drop spans have relatively good prediction when compared to the experimental error of 1%.

**Table II. RMSE and rRMS for the BFBT Series 6 two-phase pressure drop results**

| Pressure Tap | RMSE [kPa] | rRMS [%] |
|---|---|---|
| dp301 | 1.596 | 19.3 |
| dp302 | 8.550 | 18.4 |
| dp303 | 0.920 | 15.0 |
| dp304 | 0.295 | 3.5 |
| dp305 | 0.336 | 4.1 |
| dp306 | 0.365 | 6.4 |
| dp307 | 0.740 | 5.2 |
| dp308 | 0.465 | 6.4 |
| dp309 | 1.676 | 2.9 |
| Total | 1.123 | 11.0 |

### 3.2.2 FRIGG

In the FRIGG simulations, the various components of the pressure drop, shown in Equation (7), are calculated and compared. These components are the frictional, acceleration, and gravitational losses. In the FRIGG experiment, the reported frictional loss is actually the total pressure drop (including acceleration and gravity) and the acceleration loss includes the gravitational effect. Figure 4 illustrates the comparison between CTF results and FRIGG measurements which were obtained by manually extracting data points from plots, which adds some uncertainty. The total pressure drop values have a respectable 6.3% average rRMS for each data point.

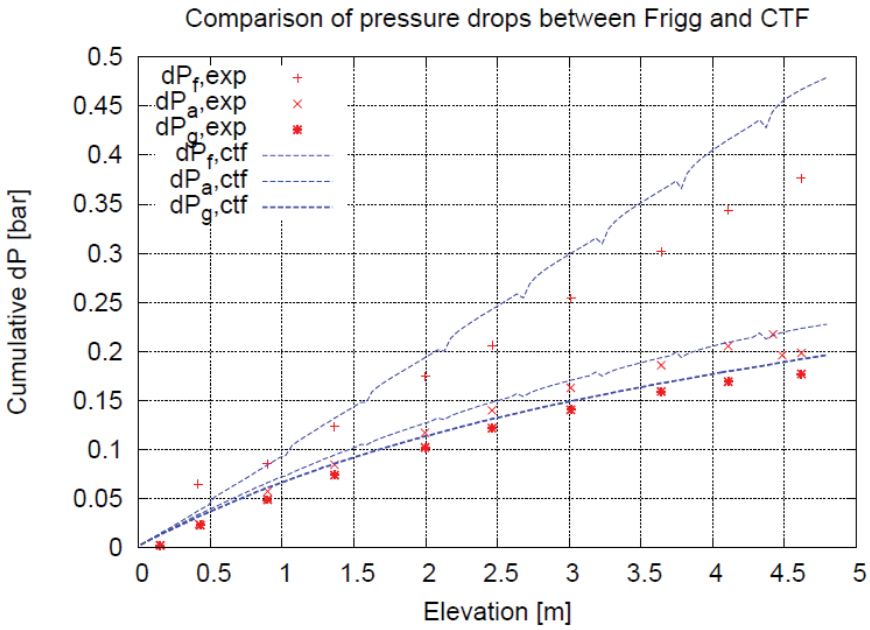


**Figure 4. FRIGG experimental vs. predicted pressure drops**

## 3.3 Void Content

Prediction of a three-dimension void distribution is one of CTF's features that is commonly used. Experimental void fraction measurements are often performed with equipment such as gamma beams that have experimental errors near 3-5% [4]. CTF utilizes its boiling equations as well as its void-drift model in order to calculate void content values of simulations. Depending on the flow regime, CTF uses different heat transfer correlations which are tied to the determination of the void content.

### 3.3.1 PSBT

Three axial locations along the PSBT bundle were analyzed during the experiments and void fraction were reported as an average of the four central subchannels within the 5x5 bundle's geometry. These three locations are labeled as the lower, middle, and upper locations. The experimental uncertainty for the Series 5, 6, and 7 test cases is reported as 4%. There are 12 test cases from Series 5, 11 from Series 6, and 12 from Series 7 selected for simulation with CTF. The RMSE of the measured and predicted void fractions for these three test series are shown in Table III. These results are all near 5%, which is just outside of the experimental error and therefore shows good prediction by CTF for these void fractions. Figure 5 shows the agreement of the CTF-predicted results against the experimentally-measured values for Series 5 with ±2σ, where the standard deviation is set as 4% error. This shows that nearly all of the points fall within the expected range and there are no extreme outliers. The most significant outliers occur in the upper portion of the PSBT geometry. This is where the void fraction is highest and therefore relies more heavily on a code's ability to predict the two-phase flow accurately.

**Table III. RMSE for the PSBT Series 5, 6, and 7 test cases**

| Location | Series 5 | Series 6 | Series 7 |
|---|---|---|---|
| Lower | 0.036 | 0.065 | 0.032 |
| Middle | 0.056 | 0.046 | 0.072 |
| Upper | 0.069 | 0.057 | 0.041 |
| Total | 0.052 | 0.056 | 0.051 |

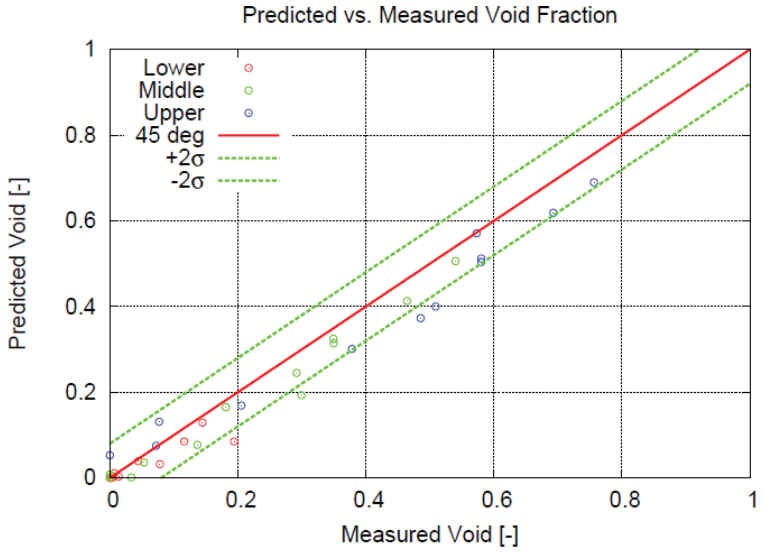


**Figure 5. PSBT Series 5 predicted vs. measured void fractions with ±4% error bars**

### 3.3.2 FRIGG

The void fraction was measured at various axial locations along the experimental setup. The CTF predictions were bundle-averaged and compared with the measurements and the results are shown in Figure 6. These predicted values follow the trend of the measured data quite well, which is important considering how high the void fraction gets at the upper elevations of the geometry.

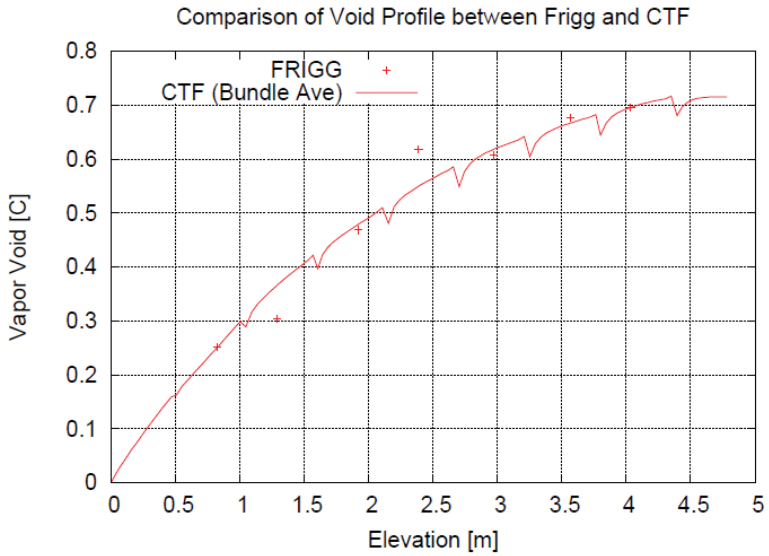


**Figure 6. FRIGG experimental vs. CTF-predicted axial void fraction**

### 3.4 Turbulent Mixing and Void Drift

CTF has void drift and turbulent mixing models that can be turned on or off via user input. These models account for inter-channel transfer of mass, momentum, and energy due to turbulence and difference in void in adjacent subchannels. CTF's segregated flow equations such as the vapor and liquid momentum and mass flow rates are updated depending on the user's choice of these models. Within CTF, turbulent mixing is modeled with a simple diffusion approximation utilizing mixing length theory acting only in the lateral directions. The turbulent mixing is separated by flow field as well as for mass, momentum, and energy. The void drift terms can be separated in the mass mixing equation to produce an equation each for the turbulent mixing coefficient, Equation (8), and for the void drift, Equation (9).

$$W_{ij,v,TM}^{D'} = -V^T \rho_g \left[\alpha_{v,j} - \alpha_{v,i}\right] \tag{8}$$

$$W_{ij,v,VD}^{D'} = V^T \rho_g \left[\left(\alpha_{v,j} - \alpha_{v,i}\right)_{\text{equil}}\right] \tag{9}$$

The turbulent transverse mixing rate for energy from subchannel *i* to subchannel *j*, similar to that found in Equation (8) (which is for mass), is then used with the gap width and the area-weighted mass flux to calculate a mixing coefficient as shown in Equation (10).

$$\beta = \frac{\text{Transverse Mass Flux}}{\text{Axial Mass Flux}} = \frac{\mathrm{W_{ij}^{H'}}/s_{ij}}{\bar{G}} \tag{10}$$

#### 3.4.1 GE 3x3

The predicted results for these test cases were run with the void drift model on, and then off. The turbulent mixing model was left on for all cases. The experimental error in the exit equilibrium quality measurements is stated as ±0.02, while the mass flux and the enthalpy are both measured to ±3.0%. It is clear from the results that the void drift model has an impact on the predicted values, as turning it off has a large impact especially on the simulated values for the corner and inner subchannels. This is largely due to the redistribution of flow that the model accounts for. These results are summarized in Table IV. Figure 7 and Figure 8 show the difference in the predictions for the exit mass flux (grouped by subchannel type) with the void drift model turned on and off, respectively. There is a notable difference, especially for the corner-type channels. With the void drift model on, almost all values fall within the ±3.0% bounds, but when the model is off the number within these error bounds falls sharply. The largest difference is visible in the corner subchannels as these have the fewest connections to heated rods and therefore are the most affected when additional mixing is allowed via the void drift model.

**Table IV. RMSE for the GE 3x3 test case results by subchannel type, void drift model on/off**

| | Exit Equilibrium Quality [-] | | Exit Mass Flux [kg/m$^2$-s] | |
|---|---|---|---|---|
| **Location** | **RMSE** [void drift **on**] | **RMSE** [void drift **off**] | **RMSE** [void drift **on**] | **RMSE** [void drift **off**] |
| Corner | 0.029 | 0.134 | 79.96 | 260.1 |
| Side | 0.016 | 0.017 | 31.22 | 42.32 |
| Inner | 0.015 | 0.036 | 38.03 | 86.27 |

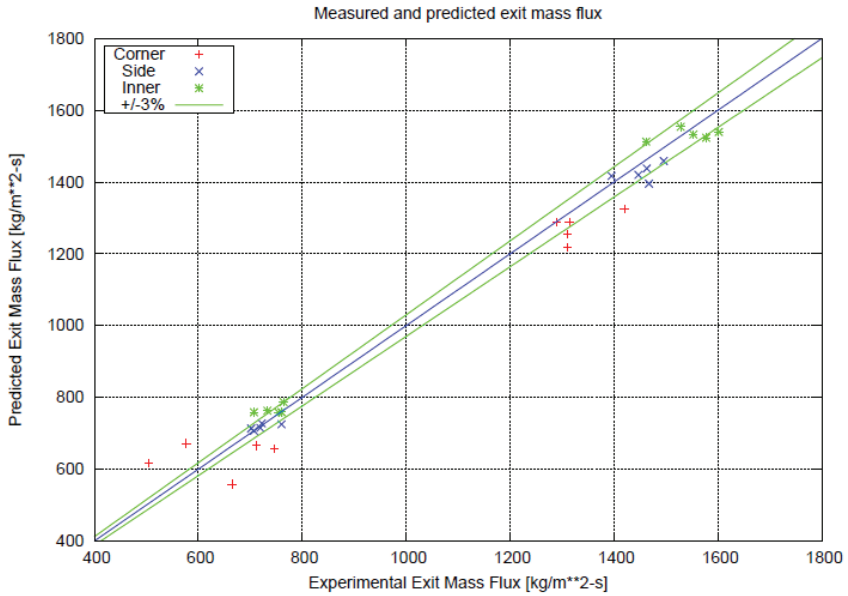


**Figure 7. GE 3x3 predicted vs. measured exit mass flux with void drift model on**

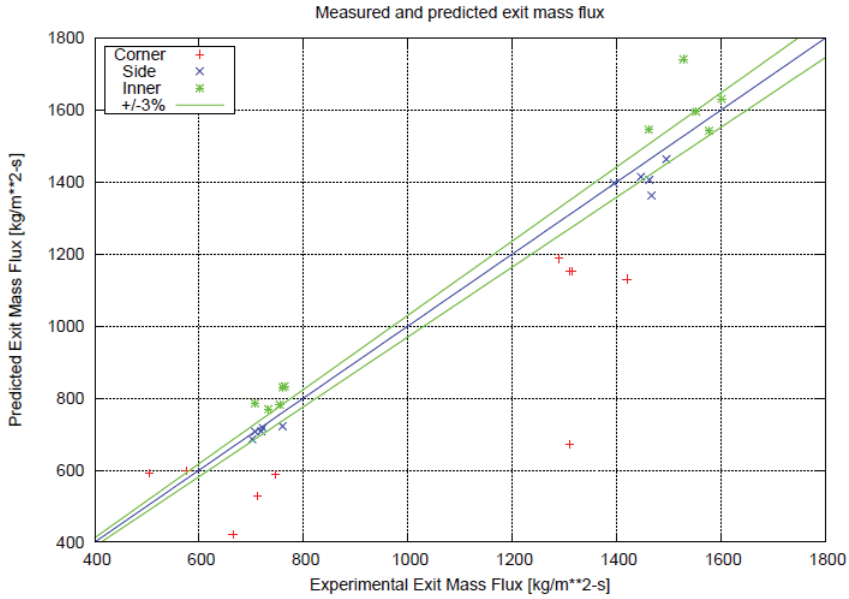


**Figure 8. GE 3x3 predicted vs. measured exit mass flux with void drift model off**

### 3.4.2 CE 5x5

Over 70 test cases of CE Test 74 were run in CTF in order to compare the subchannel exit fluid temperatures. The spacer grids contained within the CE 5x5 geometries were included in the CTF input and applied on a per-channel basis. The average differences between the CTF-predicted values and the measured values for each of the 36 subchannels are shown in Figure 9. There is no real discernible pattern for these results, but the largest deviations appear to fall in the corner and side subchannels. CTF is, on average, within 10 °F with its simulations of the CE test cases, with a general trend of over-prediction by around 2 °F. The measurement error is reported to be 0.5 °F for the thermocouples [7]. The thermocouples were placed in the center of the subchannels whereas CTF provides a subchannel-averaged temperature. In this respect the CTF values are expected to be higher as they include the effect of the hot

fluid near the rod surfaces as well. Figure 10 shows the average differences grouped by subchannel type, and here it is more apparent that the side and corner subchannels have, on average, a larger deviation from the expected results than the inner subchannels.

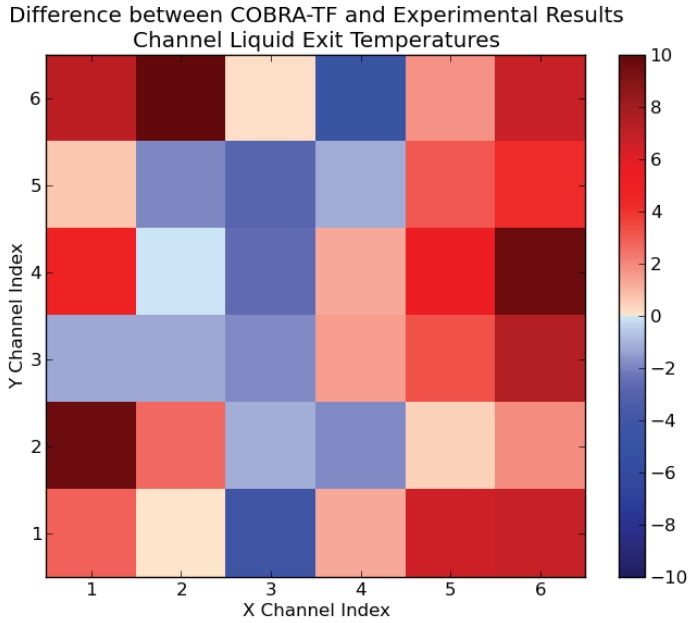


**Figure 9. Average difference [°F] between the predicted and measured exit fluid temperatures by subchannel location**

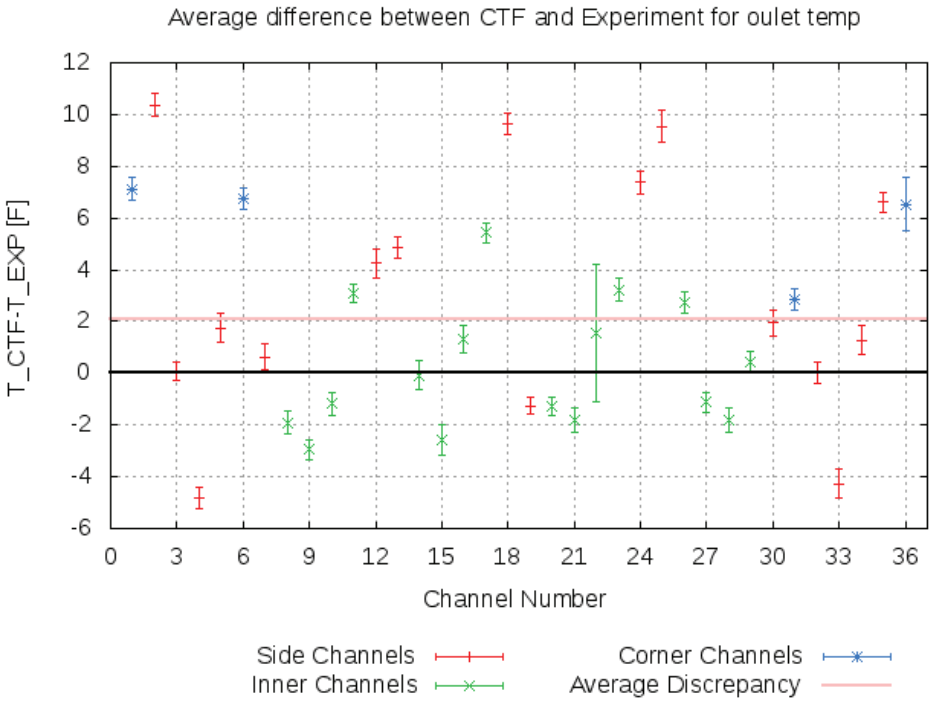


**Figure 10. Average in difference [°F] between the predicted and measured exit fluid temperatures by subchannel type and index**

## 3.5 Heat Transfer

A main objective of CTF with respect to heat transfer is to accurately predict the applicable Heat Transfer Coefficient (HTC). A code must back-calculate the HTC using relevant temperatures such as those of the bulk fluid and the wall or rod surface. Equation (11) shows Newton's law of cooling.

$$q'' = h(T_w - T_b) \tag{11}$$

Since the bulk fluid temperature must often be predicted, it is sometimes more practical and meaningful to directly compare the wall temperature to the measured surface temperatures, if available.

### 3.5.1 CE 5x5

The rod surface temperature prediction capabilities can be exercised by using the results of the test cases from the CE 5x5 experiments. Four thermocouples were placed azimuthally around select rods and the resulting temperature measurements are compared with predictions from CTF. These types of simulations are important as they show that CTF can accurately generate temperatures at the fluid-rod interface, which is a complex area to model. The results from Rod 25, the central heated rod, are shown in Figure 11. These results are grouped by the thermocouple position as well as the axial location of the surface temperature measurements. The vertical blue lines indicate the position of a spacer grid, and the thermocouple readings are slightly offset axially in order to aid in reading the data from the figure. The predictions are on average within 10 °F and the standard deviation of the differences is not too large. The predicted values are all lower than the experimental values, which could be due to over-prediction of the heat transfer coefficient from the rod to the fluid. The azimuthal differences (each of the four thermocouples is at a different circumferential location) are due to the mixing-vane grid in the geometry, which cannot be properly accounted for by CTF due to their azimuthal variations. The grid-enhancement model was not utilized, which would cause under-prediction of heat transfer downstream of the grid. The overall results show that CTF is over-predicting, however.

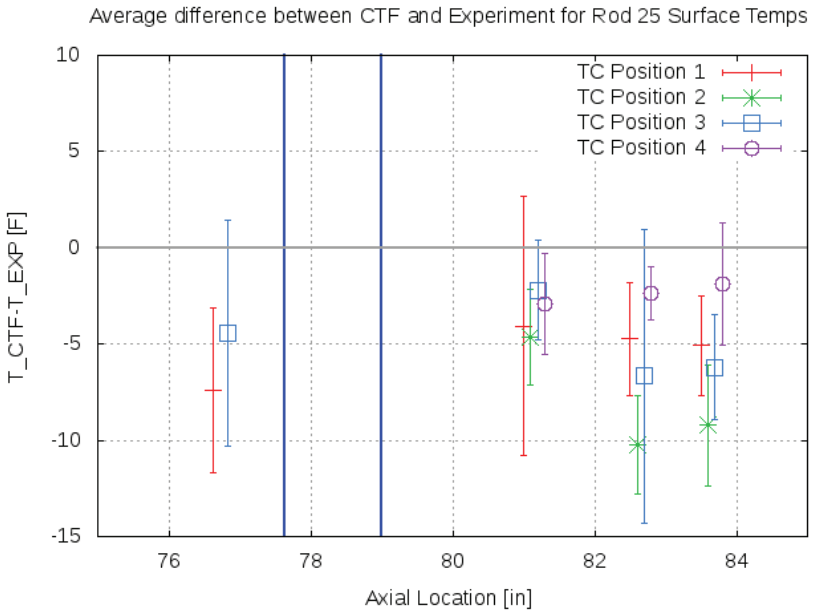


**Figure 11. Average temperature differences between predicted and measured rod surface temperatures of Rod 25**

## 3.6 Natural Circulation

This portion of experiments tests CTF's ability to replicate flow conditions which are mainly or entirely driven by buoyancy found in natural circulation around heated rods. These often involve low

system pressure, temperature, and flow rate. These boundary conditions test a subchannel code's flexibility in modeling. CTF can struggle to converge on a solution when the system pressure is low. In order to aid in convergence this parameter may be slightly altered without drastically altering the fluid properties used in the calculations.

### 3.6.1 PNNL 2x6

The CTF model for the PNNL 2x6 experiments includes the 12 rods and 21 subchannels as shown in Figure 1, broken down axially into 30 nodes at 2 inches per node. This accounts for 6 inches of unheated rods both above and below the 48 inch heated length. CTF's second rod friction option ($\lambda = 0.204Re^{-0.2}$) was utilized, and the single-phase mixing coefficient was set to the Rogers and Rosehart correlation. Since these are single-phase cases, the liquid entrainment, two-phase mixing, and void drift options were turned off or left as default. The system pressure of the CTF simulation was raised to 60 psi in order to achieve convergence---fluid properties at this pressure do not substantially deviate from those at atmospheric pressure.

CTF shows its ability to model buoyancy-driven natural circulation when using the data from the PNNL 2x6 steady-state experiment. Temperature and velocity measurements were taken and CTF's predictions of these flow patterns show good agreement for the most part. There are windows spaced along the heated length through which measurements were made. The left half of the geometry is heated while the right is adiabatic, and the water inlet is near room temperature and at a very low flow rate. Figure 12 shows the temperature difference for both the measured and predicted values at the upper-most window. The results are shown as relative to the difference between the outlet and inlet temperatures. In actuality, since the entire left side of the geometry is heated, there is no reason why the measured results should show a decrease in temperature on the left. The authors note this but do not offer an explanation. Otherwise, CTF matches closely to the low-flow and low-temperature case.

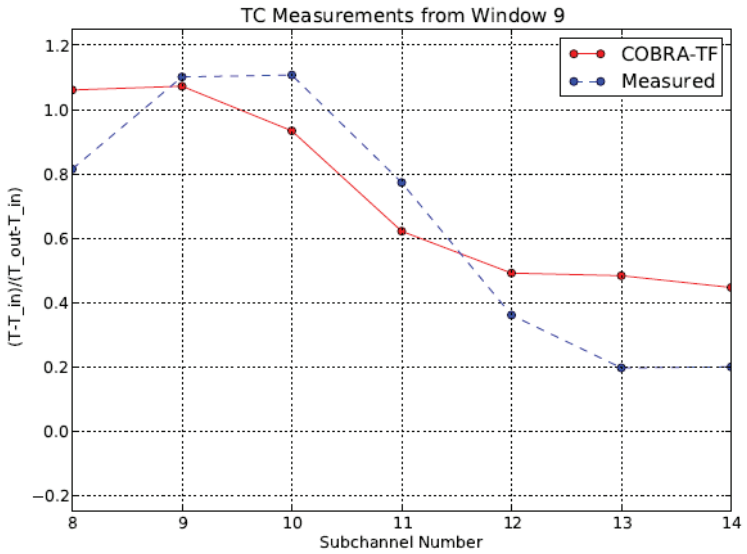


**Figure 12. PNNL window 9 predicted vs. measured subchannel-center relative temperature differences**

## 4 CONCLUSION

This document provides a brief summary of the types of validation procedures that are currently implemented with some of CTF's predictive abilities to ascertain accuracy in its calculations. Code validation is an important step of code development and expansion. CTF's most important features, such as pressure drop, void fraction, rod/coolant temperature, and mixing predictions, are all tested with the

experimental data discussed in this document. A thorough testing matrix is required to assess CTF's qualitative and quantitative abilities and accuracy. Currently, not all of CTF's features are tested with measured results, but those that are have shown that CTF can meet the requirements of a thermal-hydraulic subchannel code. At this time there are no comparisons with other subchannel codes made in this document to show how CTF compares with relevant codes running the same experiments. This type of comparison could illuminate where CTF's current strengths and weaknesses lie.

As the capabilities of CTF grow, more experimental data against which numerical results can be compared will be required. Running a validation test suite with carefully-chosen test cases during code development ensures that new procedures and options to the code are in line with expected results and that capabilities are not compromised during source alterations. Meaningful QOI predictions which are validated with experimental data together with a well-documented code provide users and developers a useful thermal-hydraulic code in CTF. Its relative accuracy for its computational time allows users to adjust the input as necessary without major computational costs. The validation efforts documented in this paper are ongoing and will continue to make use of available data to provide a means of comparison between predicted and measured results.

## 5 ACKNOWLEDGMENTS

This research is supported by and performed in conjunction with the Consortium for Advanced Simulation of Light Water Reactors (http://www.casl.gov), an Energy Innovation Hub (http://www.energy.gov/hubs) for Modeling and Simulation of Nuclear Reactors under U.S. Department of Energy Contract No. DE-AC05-00OR22725.

## 6 REFERENCES

1. R. Salko et al., "CTF Validation," CASL-U-2014-0169-000, 2014.
2. M. Avramova, "CTF: A Thermal Hydraulic Sub-Channel Code for LWR Transient Analyses, User's Manual," 2009.
3. B. Neykov, F. Aydogan, L. Hochreiter, K. Ivanov, H. Utsuno, and F. Kasahara, "NUPEC BWR Full-size Fine-mesh Bundle Test (BFBT) Benchmark," Nuclear Energy Agency, 2006.
4. A. Rubin, A. Schoedel, M. Avramova, H. Utsuno, S. Bajorek, and A. Velazquez-Lozada, "OECD/NRC Benchmark Based on NUPEC PWR Subchannel and Bundle Tests (PSBT)," US NRC and OECD Nuclear Energy Agency, 2010.
5. J. M. Bates and E. U. Khan, "Investigation of Combined Free and Forced Convection in a 2x6 Rod Bundle during Controlled Flow Transients," PNL-3135, Battelle Pacific Northwest Laboratories, 1980.
6. M. S. Quigley, C. A. McMonagle, and J. M. Bates, "Investigation of Combined Free and Forced Convection in a 2x6 Rod Bundle," BNWL-2216, Battelle Pacific Northwest Laboratories, 1997.
7. Z. Karoutas, Y. Sung, Y. Chang, G. Kogan, and P. Joffre, "Subcooled Boiling Data from Rod Bundles," EPRI Report 1003383, 2002.
8. D. W. Radcliffe, R. T. Lahey Jr., B. S. Shirlakar, "Two-Phase Flow and Heat Transfer in Multirod Geometries: Subchannel and Pressure Drop Measurements in a Nine-Rod Bundle for Diabatic and Adiabatic Conditions," General Electric, 1970.
9. O. Nylund, K. M. Briker, R. Eklund et al., "FRIGG Loop Project,", R4-447/RTL-1007, AB Atomenergi, Stockholm, 1968.
10. R. Salko and M. Avramova, "CTF Theory Manual," The Pennsylvania State University, 2014.